molecules

MDPI

Article

Synthesis and Antibacterial Properties of Oligomeric Dehydrogenation Polymer from Lignin Precursors

Xin Wei [1], Sheng Cui [1] and Yimin Xie [1,2,*]

[1] Research Institute of Pulp and Paper Engineering, Hubei University of Technology, Wuhan 430068, China; wxpaper123@163.com (X.W.); cui2019hbut@163.com (S.C.)
[2] Hubei Provincial Key Laboratory of Green Materials for Light Industry, Hubei University of Technology, Wuhan 430068, China
* Correspondence: ppymxie@163.com or ppymxie@hbut.edu.cn

Abstract: The lignin precursors of coniferin and syringin were synthesised, and guaiacyl-type and guaiacyl-syringyl-type oligomeric lignin dehydrogenation polymers (DHP and DHP-GS) were prepared with the bulk method. The carbon-13 nuclear magnetic resonance spectroscopy showed that both DHP-G and DHP-GS contained β-O-4, β-5, β-β, β-1, and 5-5 substructures. Extraction with petroleum ether, ether, ethanol, and acetone resulted in four fractions for each of DHP-G (C_{11}–C_{14}) and DHP-GS (C_{21}–C_{24}). The antibacterial experiments showed that the fractions with lower molecular weight had relatively strong antibacterial activity. The ether-soluble fractions (C_{12} of DHP-G and C_{22} of DHP-GS) had strong antibacterial activities against *E. coli* and *S. aureus*. The C_{12} and C_{22} fractions were further separated by preparative chromatography, and 10 bioactive compounds (G_1–G_5 and GS_1–GS_5) were obtained. The overall antibacterial activities of these 10 compounds was stronger against *E. coli* than *S. aureus*. Compounds G_1, G_2, G_3, and GS_1, which had the most significant antibacterial activities, contained β-5 substructures. Of these, G_1 had the best antibacterial activity. Its inhibition zone diameter was 19.81 ± 0.82 mm, and the minimum inhibition concentration was 56.3 ± 6.20 μg/mL. Atmospheric pressure chemical ionisation mass spectrometry (APCI-MS) showed that the antibacterial activity of G_1 was attributable to a phenylcoumarin dimer, while the introduction of syringyl units reduced antibacterial activity.

Keywords: lignin; dehydrogenation polymerisation; antibacterial property; oligomer; chemical structure

Citation: Wei, X.; Cui, S.; Xie, Y. Synthesis and Antibacterial Properties of Oligomeric Dehydrogenation Polymer from Lignin Precursors. *Molecules* **2022**, *27*, 1466. https://doi.org/10.3390/molecules27051466

Academic Editors: Daniele Castagnolo, Jürgen Brem, Mark G. Moloney and Sónia Silva

Received: 13 January 2022
Accepted: 17 February 2022
Published: 22 February 2022

1. Introduction

Lignin is one of the most abundant natural materials in the world, accounting for about a quarter of wood tissue, and is therefore a promising renewable material [1–3]. This highly branched aromatic polymer is a natural macromolecular compound with an amorphous structure formed by dehydrogenation and polymerisation of three phenylpropane structural monomers: sinapyl alcohol, coniferyl alcohol, and *p*-coumaryl alcohol [4–6]. Lignin mainly exists in the cell walls of plants and has good antioxidant and antibacterial properties [7–11]. Its antibacterial properties help to reduce the risk of bacterial colonisation on the surface of materials [12]. Lignin and its derivatives are considered good candidate materials for medicine and health care.

Domínguez-Robles et al. [13] prepared a composite of softwood kraft lignin and polybutylene succinate (PBS) that was resistant to the adhesion of *S. aureus*, achieving a reduction in bacterial adhesion of approximately 90% compared to PBS. Kaur et al. [14] chemically modified bagasse lignin through acetylation, epoxidation, and hydroxymethylation reactions. They found that among the modified lignin samples, epoxy lignin had the most effective antibacterial activity, with minimum inhibitory concentrations (MIC) against *Bacillus aryabhattai* and *Klebsiella* of 90 and 200 μg/mL, respectively, demonstrating that lignin has great potential for antibacterial applications. Moreover, the structure and biological activity of lignin are greatly affected by the separation and extraction methods used as

well as the molecular weight of the obtained product [15–17]. Furthermore, Rocca et al. [18] synthesised lignin-doped silver and gold nanoparticles by one-pot thermochemical and photochemical methods, and they found that the nanoparticles had a certain inhibitory effect on *E. coli* and *S. aureus*. More importantly, the particles are non-cytotoxic towards human cells at the bactericidal concentrations. Marulasiddeshwara et al. [19] also found that lignin capped silver nanoparticles (LCSN) not only have antioxidant and antibacterial properties, but also did not lyse red blood cell (RBC) membrane when assayed hemolytic activity suggested its non-toxic nature. Lourencon et al. [20] used eucalypt kraft lignin fractionated at pHs 9, 7, 5, and 3 by sequential acid precipitation. Fractions precipitated at pHs 9 and 7 have shown an outstanding antibacterial activity against five bacteria. Moreover, fractions 7 and 5 presented at cytotoxicity tests ability to inhibit the growth of U87MG and T98G glioma cells, while only a slight inhibition of adult human fibroblasts was detected. There studies show that lignin has a broad application prospect biological activity.

Enzymatically-synthesised dehydrogenation polymer is one of the most widely accepted lignin model compounds and the best lignin substitute used in various experiments. Its properties are highly similar to natural lignin [21]. In the process of synthesising DHP, the reaction conditions can be artificially controlled to adjust the type of DHP produced [22,23]. Therefore, DHP has a low degree of polymerisation, simple structure, and connectivity, and more functional groups can be obtained, which can achieve higher biological activity than natural lignin [24–26].

Ye et al. [27] synthesised DHP with isoeugenol as a monomer and found that β-O-4, β-β, β-5, and β-1 were the main structures of DHP. Its structure was similar to natural lignin. Chen et al. [28] also used isoeugenol to synthesise DHP and found that the antioxidant activity IC_{50} of the ether soluble component was 0.12 g/L. However, these studies focus on the direction of the chemical structure rather than the biological activity, and there are structural differences between isoeugenol and coniferin [29–31]. Therefore, it is more representative to synthesise oligomeric DHP with the lignin monomer coniferin, syringin, and *p*-coumaryl alcohol glucoside as precursors.

To investigate the antibacterial activity of oligomeric DHP, coniferin and syringin were used as raw materials under β-glucosidase and laccase catalysis to synthesise G-type lignin dehydrogenation polymer (DHP-G) and GS-type lignin dehydrogenation polymer (DHP-GS). The DHPs were extracted with different organic solvents and their growth inhibition effects on *E. coli* and *S. aureus* were determined by the filter paper agar diffusion method. The ether extractives C_{12} and C_{22}, which had high antibacterial activity, were further screened and purified by preparative chromatography. The obtained compounds G_1, G_2, G_3, and GS_1 were structurally identified by atmospheric pressure chemical ionisation mass spectrometry (APCI-MS). The source of their biological activity was discussed by analysing the relationship between structure and antibacterial effect.

2. Results and Discussion

2.1. ^{13}C-NMR Spectral Analysis of DHPs

The ^{13}C-NMR spectrum of DHP-G is shown in Figure 1. The weak signal peak at 190.9 ppm (No. 1) is an α-CHO produced by some oxidation during DHP polymerisation [32]. At 172.2 ppm (No. 2), the signal indicates oxidation at the γ-position to form cinnamic acid [33,34]. The signals at 149.8 to 147.0 ppm (No. 4–8) are attributable to the carbon atoms on the guaiacyl aromatic ring, and the signal at 143.6 ppm (No. 9) comes from the C4 of the 5-5 structure. The signals near 130 ppm (No. 10–14) indicate Cα/Cβ from C=C produced by the double bond on the side chain of coniferin and syringin. The signal at 87.2 (No. 20) is the Cα from the β-5 structure [35–38]. The signals at 67.2 ppm (No. 27) is the Cγ from the β-5 structure [22]. The signals at 70.2 ppm (No. 26), 85.1 ppm (No. 21), and 62.0 ppm (No. 29) are from the Cα, Cβ, and Cγ of the β-O-4 structure [39]. The signal at 63.5 ppm (No. 28) is from the Cα of the β-1 structure. The signals at 53.5 ppm (No. 31) and 46.0 ppm (No. 32) are attributed to the Cβ of the β-β structure [35,40]. These results indicate that

DHP-G mainly includes β-5 and β-O-4 structures, but also includes some 5-5, β-1, and β-β structures.

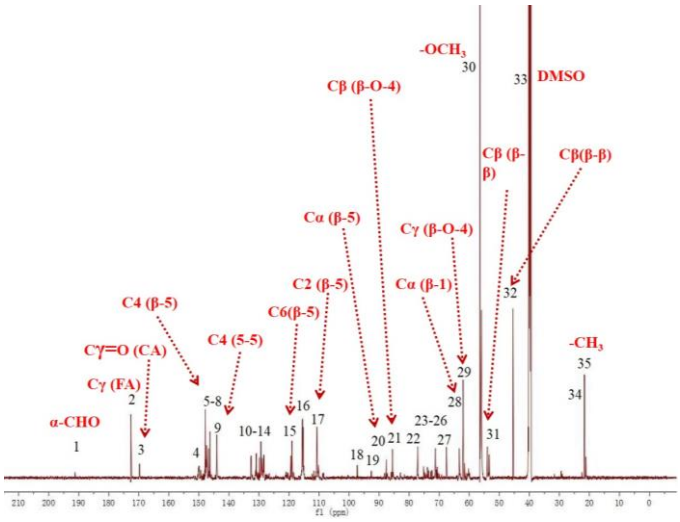

Figure 1. ^{13}C-NMR spectrum of DHP-G.

The ^{13}C-NMR spectrum of DHP-GS in Figure 2 is similar to the ^{13}C-NMR spectrum of DHP-G in Figure 1, both of which are based on β-5 and β-O-4 structures while also including 5-5, β-1, and β-β structures. The difference is that DHP-GS contains some signals generated by syringyl units. For example, the signal at 152.8 ppm (No. 4′) comes from C3 and C5 on etherified syringyl units, while DHP-G does not have these structures [41,42].

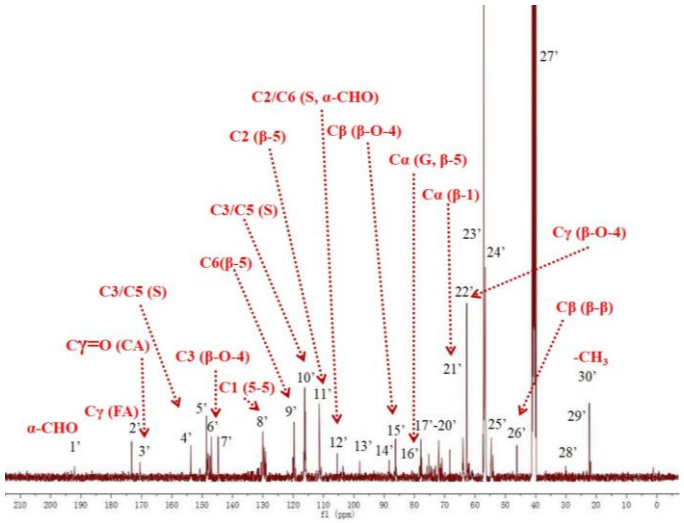

Figure 2. ^{13}C-NMR spectrum of DHP-GS.

2.2. Molecular Weight Analysis of DHP

The average molecular weights of the DHP fractions are shown in Table 1. The molecular weights of the DHP fractions increase with the enhancement of solubility of the solvent. Based on the molecular weight of coniferyl alcohol (180 Da) and the molecular weight of sinapyl alcohol (210 Da), the average molecular weights of the petroleum ether fractions C_{11} and C_{21} are 289 and 293 Da, respectively. These values are lower compared to coniferyl and sinapyl alcohol dimer, indicating that there were more monomer structures in the petroleum ether fractions.

Table 1. Average molecular weight of DHP fractions.

DHP Fractions	M_w	M_n	PDI
C_{11}	289	192	1.51
C_{12}	619	387	1.60
C_{13}	1527	988	1.55
C_{14}	2846	1923	1.48
C_{21}	293	181	1.62
C_{22}	677	462	1.47
C_{23}	1478	860	1.72
C_{24}	2642	1794	1.47

Legend: M_w: weight average molecular weight; M_n: number average molecular weight; PDI: polymer dispersity index; C_{11}: petroleum ether-extracted fraction from DHP-G; C_{12}: ether-extracted fraction from DHP-G; C_{13}: ethanol-extracted fraction from DHP-G; C_{14}: acetone-extracted fraction from DHP-G; C_{21}: petroleum ether-extracted fraction from DHP-GS; C_{22}: ether-extracted fraction from DHP-GS; C_{23}: ethanol-extracted fraction from DHP-GS; C_{24}: acetone-extracted fraction from DHP-GS.

2.3. Analysis of Antibacterial Properties of DHP Fractions

The inhibitory effects of DHP fractions, DHP precursors, and sample solvents on the growth of *E. coli* and *S. aureus* are shown in Figures 3 and 4. The antibacterial effect of the sample was evaluated by the diameter of the inhibition zone, which is shown in Figure 5. While DHP precursor and sample solvent had no obvious inhibitory effect on the growth of the two tested bacteria, all DHP fractions had different inhibitory effects on the two tested bacteria. The petroleum ether-extracted fraction and the ether-extracted fraction, which had lower molecular weights, had better growth inhibition effects on the two tested bacteria than the ethanol-extracted and acetone-extracted fractions, indicating that the molecular weight may have a certain impact on the antibacterial performance of DHP. The ether-extracted fraction had the most obvious effect on the two tested bacteria. The diameters of the inhibition zone of the ether-extracted fraction of DHP-G on *E. coli* and *S. aureus* were 13.67 ± 0.21 mm and 14.34 ± 0.28 mm, respectively, compared to 11.67 ± 0.24 mm and 12.07 ± 0.19 mm for the ether-extracted fraction of DHP-GS. The minimum inhibitory concentration (MIC) of each fraction of DHP for the two tested bacteria is shown in Figure 6. The effect of the ether-extracted fraction on the two tested bacteria was the most obvious, as the MICs of the ether-extracted fraction C_{12} of DHP-G for *E. coli* and *S. aureus* were 138.90 ± 10.70 mg/L and 89.40 ± 6.50 mg/L, respectively. The MICs of the ether-extracted fraction C_{22} of DHP-GS for *E. coli* and *S. aureus* were 216.20 ± 11.30 mg/L and 185.10 ± 12.40 mg/L, respectively.

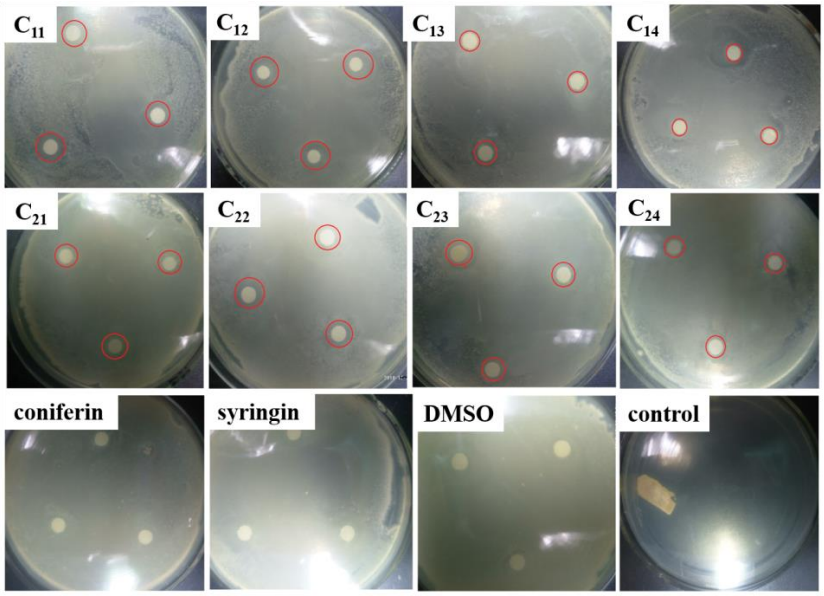

Figure 3. Effect of DHP fractions on growth inhibition of *E. coli*. Legend: The red circle area is the inhibition zone; coniferin and syringin: precursors of DHP; DMSO: No sample was added, only DMSO was added; control: control group without sample and solvent.

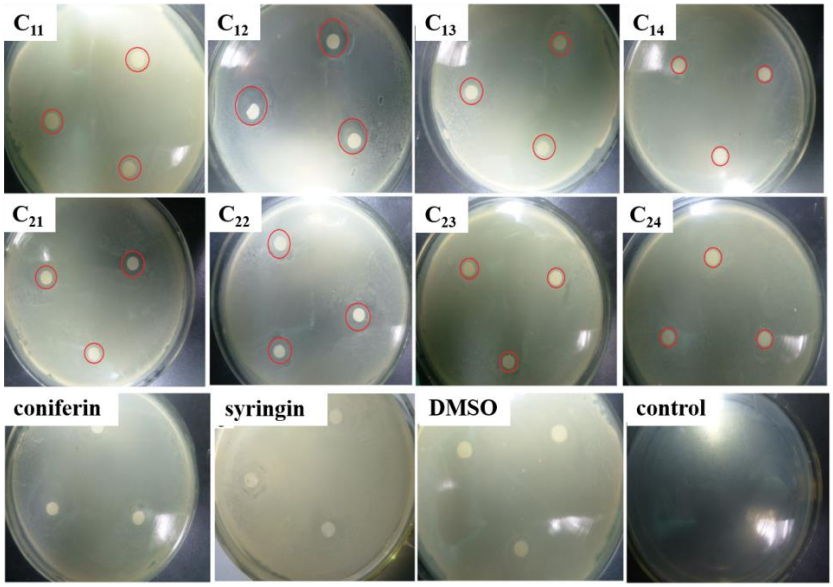

Figure 4. Inhibitory effect of DHP fractions on the growth of *S. aureus*. Legend: The red circle area is the inhibition zone; coniferin and syringin: precursors of DHP; DMSO: No sample was added, only DMSO was added; control: control group without sample and solvent.

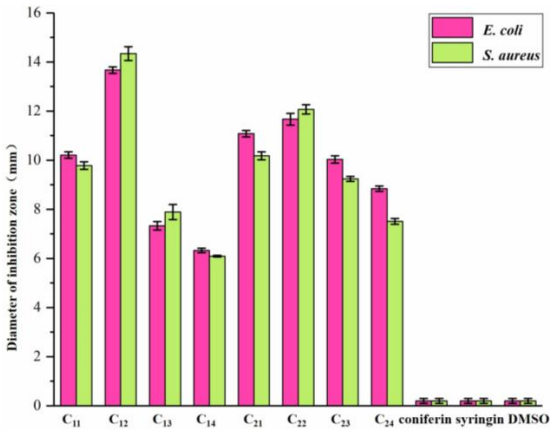

Figure 5. Inhibition zone diameter of DHP fractions on *E. coli* and *S. aureus*.

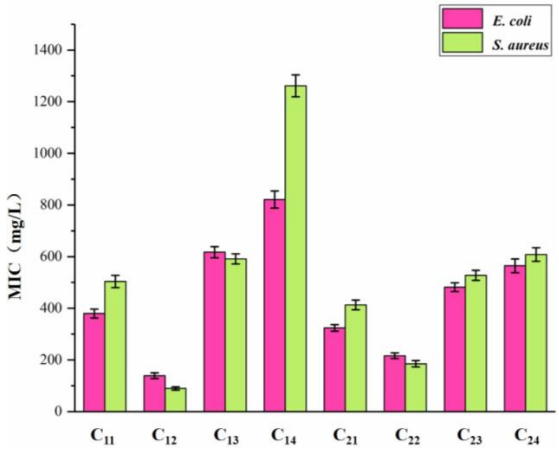

Figure 6. MIC of DHP fractions against *E. coli* and *S. aureus*. Legend: MIC: the minimum inhibitory concentration.

2.4. Analysis of Antibacterial Properties of Purified Components of DHP

The inhibitory effects of purified DHP compounds on the growth of *E. coli* and *S. aureus* are shown in Figures 7 and 8. The diameter of the inhibition zone is shown in Figure 9. The MICs are shown in Figure 10. In general, the antibacterial activities of purified compounds of the ether fractions C_{12} and C_{22} (G_1–G_5 and GS_1–GS_5) were stronger against *E. coli* than against *S. aureus*. Among the purified compounds of DHP-G, G_1 had the best inhibitory effect on the two tested bacteria. The diameters of the inhibition zone for *E. coli* and *S. aureus* were 19.81 ± 0.82 mm and 13.16 ± 0.29 mm, respectively, while the MICs were 56.30 ± 6.20 μg/mL and 146.50 ± 9.40 μg/mL, respectively. Among the purified compounds of DHP-GS, the compound GS_1 had the best inhibitory effect on the two tested bacteria, and the diameters of the inhibition zone for *E. coli* and *S. aureus* were 12.72 ± 0.21 mm and 11.42 ± 0.21 mm, respectively, with MICs of 162.50 ± 12.20 μg/mL and 229.00 ± 12.50 μg/mL, respectively.

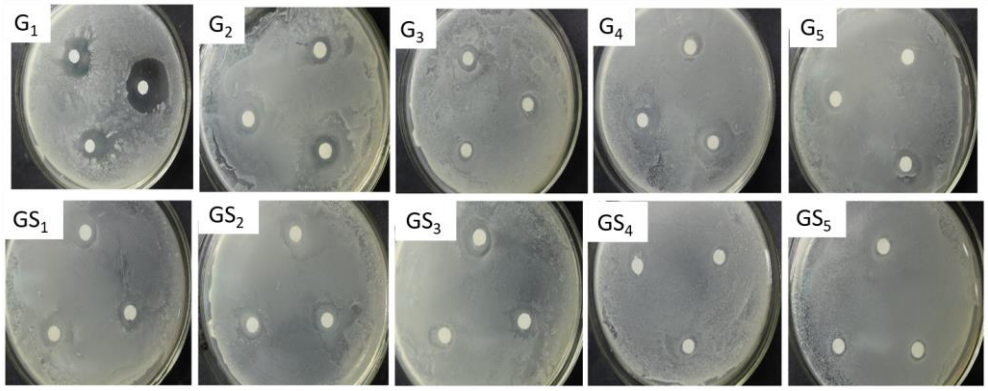

Figure 7. Inhibitory effect of purified compounds from DHP on the growth of *E. coli*. Legend: G_1–G_5: compounds purified from the ether fraction of DHP-G by preparative chromatography; GS_1–GS_5: compounds purified from the ether fraction of DHP-GS by preparative chromatography.

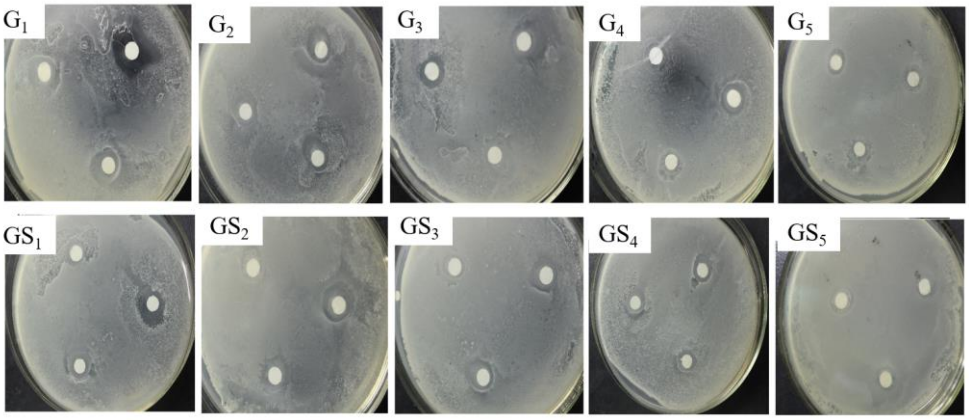

Figure 8. Inhibitory effect of purified components from DHP on the growth of *S. aureus*. Legend: G_1–G_5: compounds purified from the ether fraction of DHP-G by preparative chromatography; GS_1–GS_5: compounds purified from the ether fraction of DHP-GS by preparative chromatography.

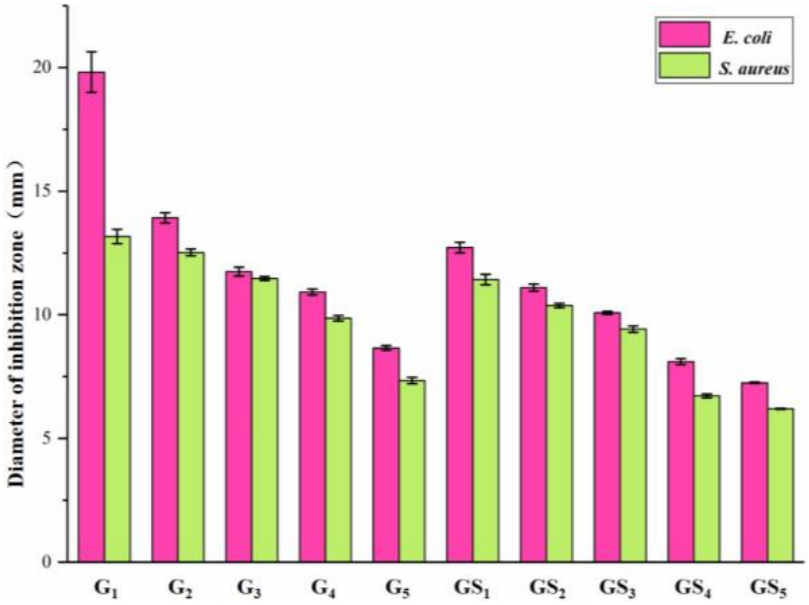

Figure 9. Inhibition zone diameter of purified compounds from DHP on *E. coli* and *S. aureus*.

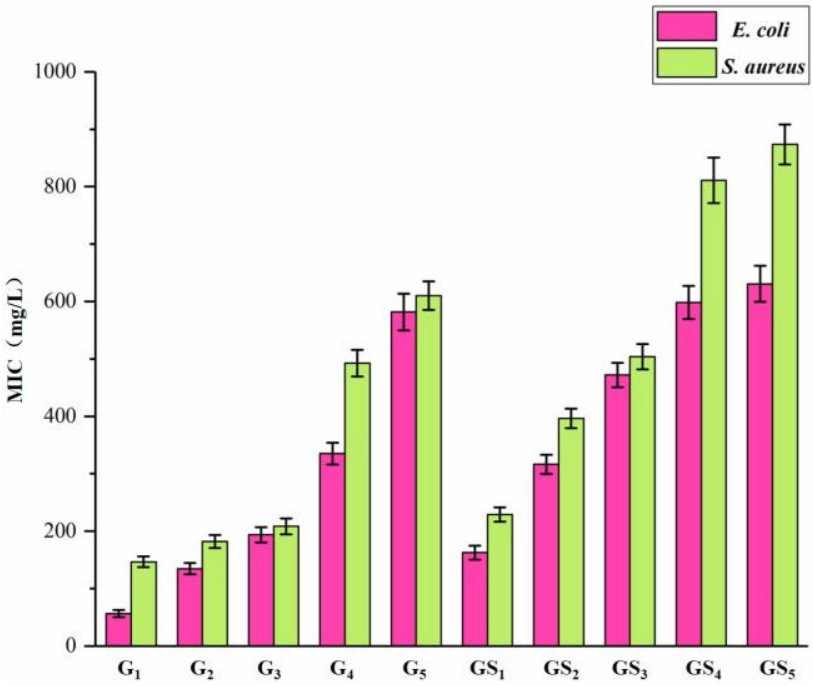

Figure 10. MIC of purified compounds from DHP against *E. coli* and *S. aureus*. Legend: MIC: the minimum inhibitory concentration.

2.5. Structural Analysis of Bioactive Purified DHP Compounds by Mass Spectrometry

The mass spectral information of G_1 is shown in Figure 11. The ionisation of the γ-position carbon in the side chain of the coniferyl alcohol monomer formed a fragment peak at m/z 149.023, while a fragment peak was formed by the cleavage of the γ-hydroxyl at m/z 163.039. The ion signal peak at m/z 279.159 was derived from the dimer of the β-5 structure. The fragment peak at m/z 341.138 came from β-5, γ-CH_2^+. From the analysis of the fragment peaks, it was found that the G1 molecular ion at m/z 357.133 was a G-type dimer (β-5, γ-CH_2OH, γ′-CH_2OH).

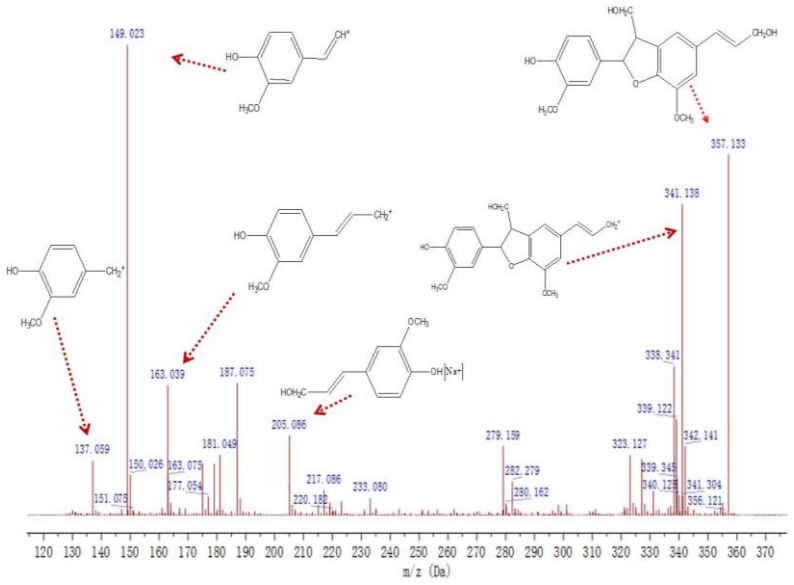

Figure 11. Mass spectrum of the compound G_1.

The mass spectral information of G_2 is shown in Figure 12. The signal at m/z 219.065 was derived from the fragmentation peak formed by the ether bond and carbon–carbon bond breakage of the coumaran ring in the phenylcoumaran structure. The signal at m/z 314.177 was from the cleavage of the carbon–carbon double bond in the side chain of the β-5 dimer. The peak at m/z 341.138 came from β-5 with γ-COOH, which acted as the precursor ion for the fragment at m/z 219.065. The signal at m/z 392.287 was generated by the capture of Na^+ by the β-5 (γ-CHOH, γ′-COOH) dimer, indicating that many monomers are polymerised through the β-5 bond, and that the side chain easily oxidised into a carboxylic acid. The molecular ion peak of G_2 appeared at m/z 564.221. According to the fragment peak analysis, the structure of G_2 is most likely a G-type trimer ((β-5)(β-5), γ-COOH, γ′-CH_2OH, γ″-COOH). The signal peak at m/z 519.201 was derived from the trimer ((β-5)(β-5), γ-COOH, γ′-CH_2OH, β″-CH^+). The loss of the carboxyl group at the γ position also confirmed the structure of G_2.

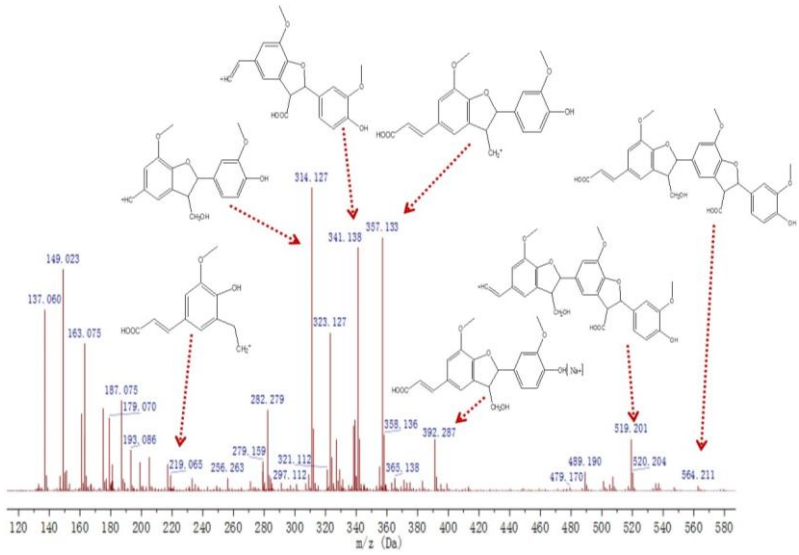

Figure 12. Mass spectrum of the compound G_2.

The mass spectral information of G_3 is shown in Figure 13. The signal peak at m/z 163.075 originated from the cleavage of the alcohol hydroxyl group at the γ position of

the coniferyl alcohol monomer. The signal at m/z 282.279 was weak and represented the signal formed by the re-fracture of the ((β-5), α-CHO) structure at m/z 311.127. The peak at m/z 490.193 originated from the cleavage of the alcoholic hydroxyl group at the γ position of the ((β-5)(β-5), γ-CH_2OH, γ′-CHO, α′-CHO) structure. The peaks at m/z 535.195 and m/z 551.211 are both attributed to the ((β-O-4)(β-5), α-OH, γ-CHO, γ′-CH_2OH, γ′′-CHO) structure. According to the fragment peak analysis, the G_3 molecular ion peak at m/z 697.263 represents a tetramer ((β-O-4)(β-5)(β-5), α-OH, γ-CHO, γ′-CH_2OH, γ′′-CHO, α′′′-CHO).

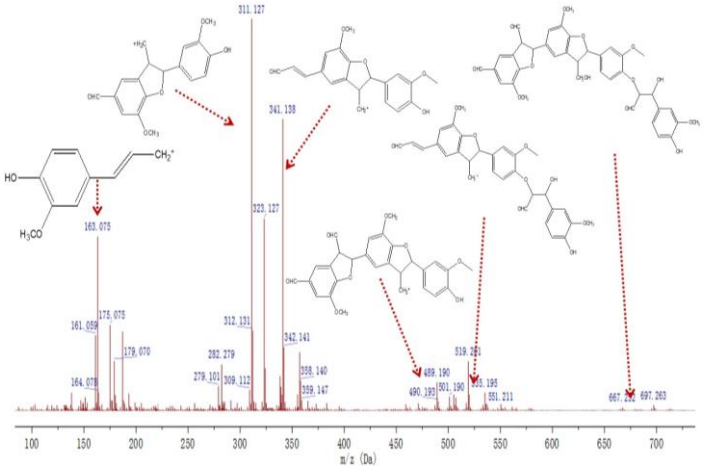

Figure 13. Mass spectrum of the compound G_3.

Figure 14 shows the mass spectral information of GS_1. The m/z 205.086 signal was a typical fragment of β-5 dimer after the cleavage of the coumaran ring. The signal at m/z 233.080 was formed by the capture of Na^+ by the sinapyl alcohol monomer. The ion peak at m/z 387.143 was derived from GS-type β-5 dimer with a detailed structure of ((β-5), γ-CH_2OH, γ′-CH_2OH). The signal at m/z 357.132 occurred due to the loss of the gamma position -CH_2OH from the fragment of m/z 387.143, indicating that the -CH_2OH at the gamma position is relatively easily lost, which again confirms the structure of GS_1.

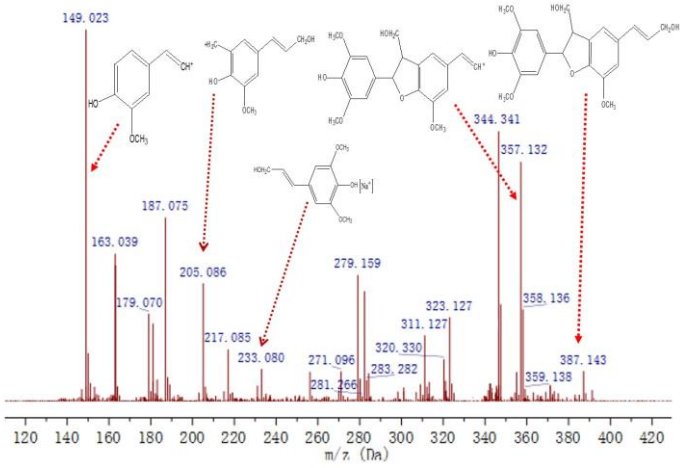

Figure 14. Mass spectrum of the compound GS_1.

According to the analyses of mass spectra, the structures of the main bioactive compounds are shown in Figure 15. Compound G_1, G_2, G_3, and GS_1, which have strong inhibitory effects on *E. coli* and *S. aureus* are demonstrated above, and all contain β-5 structures. Differences in the antibacterial activities of these compounds mainly depended on the degree of polymerisation. The G_1 is a G-type dimer (β-5, γ-CH_2OH, γ′-CH_2OH),

and the G_2 is a G-type trimer ((β-5)(β-5), γ-COOH, γ′-CHOH, γ″-COOH), while the G_3 is a G-type tetramer ((β-O-4)(β-5)(β-5), α-OH, γ-CHO, γ′-CH_2OH, γ″-CHO, α‴-CHO). Thus, as the molecular weight increased, the antibacterial activity of the compound was reduced to a certain extent. Xie et al. [43] found that the total phenol content which was related with antibacterial properties of DHPs decrease with the increase in their molecular weights. On the other hand, as compared with higher molecular weight substances, substances with lower molecular weight can easily penetrate the cell membrane of bacteria to have a better antibacterial effect. This result explains the phenomenon well, and some other researchers have similar findings [44–47].

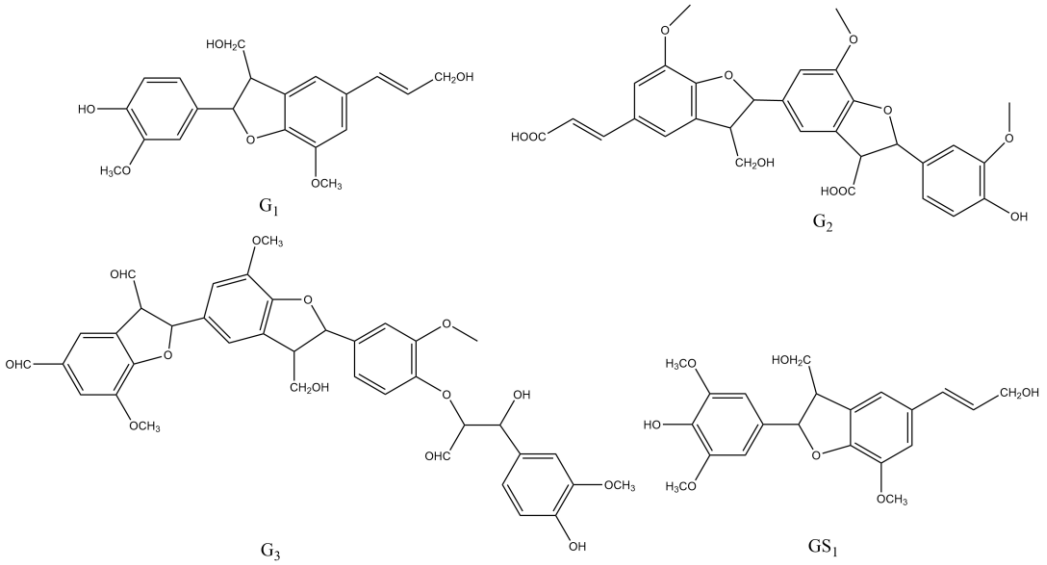

Figure 15. Chemical structure of the compound G_1, G_2, G_3, and GS_1 with significant antibacterial effects.

The GS_1 compound has an additional methoxy group at the fifth position of the S-type monomer compared to the G_1, but the antibacterial activity of GS_1 was significantly weaker than that of the G_1. The syringyl structure reduced the antibacterial properties of the substance. Shaikh et al. [48] synthesised 14 coumaran derivatives, most of which were active against *Mycobacterium tuberculosis* (H37Rv), and found that the MICs of some compounds for *S. aureus*, *Bacillus* sps., and *E. coli* strains were as low as 0.8–1.6 μg/mL, while the MICs for *Candida albicans*, *Aspergillus flavus*, *Aspergillus niger*, and *Aspergillus fumigatus* were as low as 0.4–6.25 μg/mL. Senioa et al. [49] prepared hydromethanolic extracts and infusions from air-dried and freeze-dried *Galium aparine* L. containing phenylcoumaran to detect biological activity, and found that the MICs of the sample against *E. coli* and *S. aureus* were 3.75–30 mg/mL and 1.85–15 mg/mL, respectively. Xie et al. [50] used isoeugenol as a precursor to synthesise a low molecular weight DHP catalysed by laccase. Its antibacterial performance may be due to the existence of its β-5 structure, which was also observed in the present study. Hattori et al. [51] fractionated of the methanolic extract of the aril of *Myristica fragrans* Houtt. Followed by microbial assay using the tube dilution technique, they found that two substances containing phenylcoumaran structure could inhibit bacterial glucosyltransferase and cause loss of bacterial adhesion, which resulted in good antibacterial properties. The remaining three substances without phenylcoumaran structure had not this ability, resulting in poor antibacterial properties. The present results were in good agreement with their findings. This provides a useful direction for the development of the antibacterial industry in the future.

3. Materials and Methods

3.1. Materials

Coniferin and syringin, as shown in Figure 16, were synthesised with vanillin and syringaldehyde, respectively [40,52]. β-Glucosidase was purchased from Sigma Co., Ltd. (Shanghai, China) and laccase (No.51003) from Novazyme Co., Ltd. (Tianjin, China). The other chemicals were of analytical grade, purchased from Sinopharm Chemical Reagent Co., Ltd. (Shanghai, China).

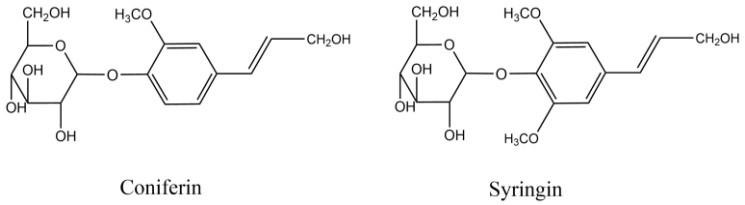

Figure 16. Chemical structure of coniferin and syringin.

Gram-negative bacteria *E. coli* ATCC 25,922 and Gram-positive bacteria *S. aureus* CMCC (B) 26,003 were purchased from Shanghai Luwei Technology Co., Ltd. (Shanghai, China). Ordinary nutrient agar culture medium was purchased from Aobox Biotechnology Company (Beijing, China) and used for agar plates, which were autoclaved at 121 °C for 30 min.

3.2. Synthesis of DHP

The chemical structure changes during the formation of DHP-G are shown in Figure 17. Coniferin (8.8 mmol) was dissolved in 0.2 mol/L sterile acetic acid/sodium acetate buffer solution (100 mL, pH 5.0), then β-Glucosidase (30 mg, 6.4 U/mg) and laccase (2 mL, 1093 IU/mL) were added with mixture. The reaction continued under sterile air filtered by activated carbon and the mixture reacted at 30 °C in a water bath for 30 min. The reaction was completed by adding 100 mL of distilled water after 30 min and heating in a water bath at 60 °C to end the reaction. The precipitated fraction was collected after centrifugation and washed with distilled water several times. After freeze-drying, the product was extracted with a mixture of dichloroethane/ethanol (2:1 *v*/*v*, 60 mL) for 6 h, and then centrifuged to collect the dissolved fraction [39]. The solvent was removed in vacuo to obtain purified DHP-G with a yield of 88.3%.

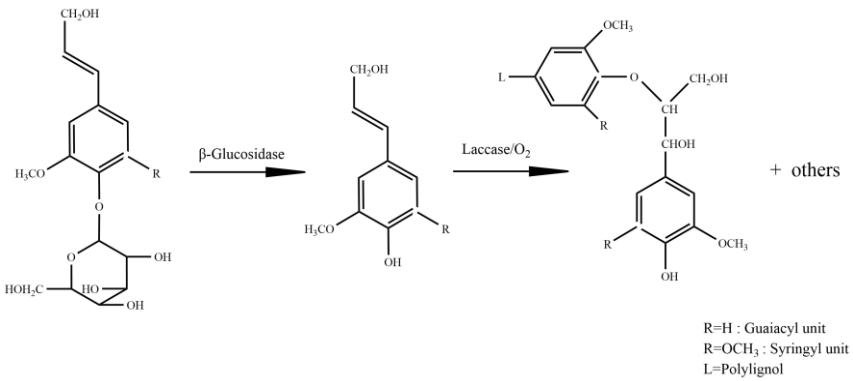

Figure 17. Chemical structure diagrams of DHP-G formation.

The synthesis of DHP-GS was consistent with the above steps, with raw material consisting of coniferin (4.0 mmol) and syringin (4.0 mmol), resulting in a yield of DHP-GS of 80.9%.

3.3. Classification of the DHP

As shown in Figure 18, classification was conducted according to the polarity and solubility of different organic solvents and referring to the methods of Wang et al. and Li et al. [53,54]. Petroleum ether, ether, ethanol, and acetone were used to fractionate DHP-G and DHP-GS. The petroleum ether fraction, ether fraction, ethanol fraction, and acetone fraction were sequentially obtained from DHP-G, and the yields were 2.1%, 26.2%, 31.3%, and 7.8%, respectively. The petroleum ether, ether, ethanol, and acetone fractions were also obtained from DHP-GS, and the yields were 2.5%, 24.3%, 40.8%, and 9.7%, respectively.

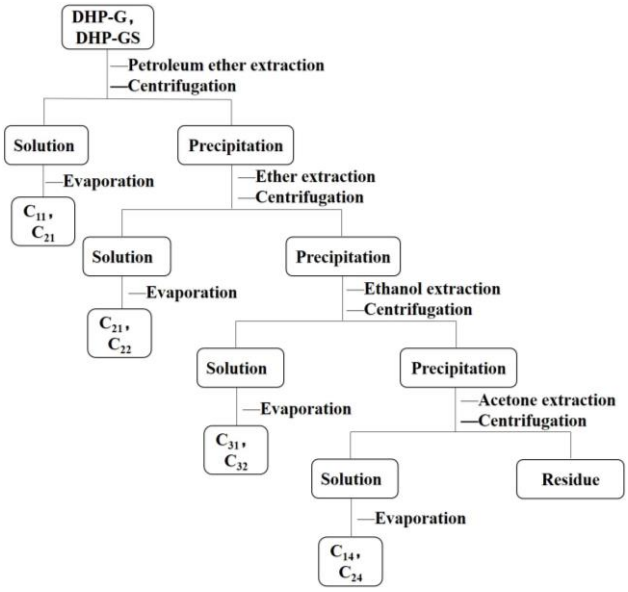

Figure 18. Classification flow chart of DHP-G and DHP-GS.

3.4. ^{13}C-NMR Measurement of DHP-G and DHP-GS

80 mg of DHP-G or DHP-GS sample was placed into a Φ 5 mm NMR tube and dissolved in 0.6 mL DMSO-d_6 (0.6 mL). A 600-dd2 NMR spectrometer (DD2-600, Agilent Technologies, Santa Clara, CA, USA) was used to scan the solution at 150.83 MHz to obtain the corresponding ^{13}C-NMR spectrum. The parameters of the instrument were: pulse delay: 2.5000 s, acquisition time: 0.9437 s, and scanning time: 6000 times.

3.5. Determination of Molecular Weight of the DHP Fractions

The relative molecular weight of each fraction of DHP was determined by size exclusion chromatography. Each DHP fraction (2 mg) was dissolved in N,N-dimethylformamide (DMF) (2 mL), filtered through a 0.22 μm microporous membrane, and then injected into a Shimadzu LC 20A gel permeation chromatograph (GPC) (LC 20A, Shimadzu, Kyoto, Japan). The separation column was a Shim-pack GPC-803D (300 mm × 8 mm) (803D, Shimadzu, Kyoto, Japan) and the mobile phase was DMF with a flow rate of 0.6 mL/min. The column temperature was 35 °C, and the injection volume was 25 μL. Polystyrene was used as the standard.

3.6. Purification of Ether Fraction of DHP with Preparative Column Chromatography

As shown in Figure 19, referring to the methods of Tan et al. and Xiang et al. [55,56], the fractions C_{12} and C_{22} with high antibacterial activity were further purified by preparative column chromatography (Biuchi C-615, Buchi Lab Equipment, Flawil, Switzerland) and eluted with acetone/n-hexane (2:3 *v*/*v*), acetone/n-hexane (3:2 *v*/*v*), or methanol/chloroform (1:18 *v*/*v*). The yields of compounds G_1 to G_5 purified from C_{12} were 39.2%, 28.7%, 15.4%, 8.9%, and 7.8%, respectively. The yields of compound GS_1 to GS_5 purified from C_{22} were 43.5%, 26.9%, 12.0%, 10.4%, and 7.2%, respectively.

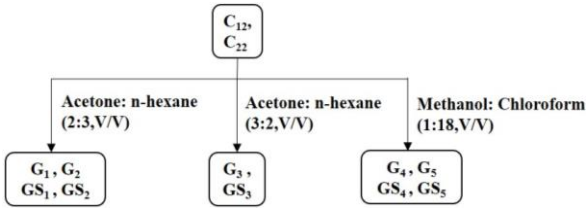

Figure 19. Purification process of DHP ether component.

3.7. Determination of the Antibacterial Activity of DHP Fractions and Purified Compounds

The antibacterial activities of fractionated DHP components and purified compounds were determined by the filter paper agar diffusion method [57–60]. The *E. coli* or *S. aureus* suspension was diluted with a McFarland turbidity of 0.5 with sterile saline, and the bacterial concentration was approximately 1.5×10^8 CFU/mL. On each agar plate, 200 µL diluted bacterial suspension were applied evenly. The sample was dissolved in dimethyl sulfoxide/normal saline (4:96 V/V, 0.1% Tween 80 as dispersant) to obtain a series of solutions with a concentration of 5 mg/mL. Dry sterile filter paper with a diameter of 6.00 mm was soaked in the above solution for 6 h, then removed and attached to the agar plate containing bacteria. Three filter paper discs were on each dish. The corresponding DHP sample solution (10 µL) was then added to the surface of the filter paper, which was incubated at 37 °C for 24 h. The diameter of the inhibition zone around the filter paper was observed and determined and the average value was calculated.

The minimum inhibitory concentration (MIC) was determined by the test tube two-fold serial dilution method, with a slight improvement [61]. Several 18 × 180 mm test tubes were prepared, and the first tube with broth medium with a concentration of 4 mg/mL and a volume of 4 mL. Then, 2 mL from the first tube was removed to the second tube and 2 mL of the corresponding solvent was added. This operation was repeated for 10 tubes; note that the last tube should also be taken out 2 mL to remove the corresponding solvent. Then, 50 µL of the diluted bacterial solution was added to each test tube and placed in the incubator for 24 h. The corresponding concentrations of non-turbid and turbid in adjacent test tubes were recorded. A series of gradient samples was prepared between the above concentrations, and bacteria solutions were added. The above steps were repeated three times to obtain more accurate MIC data and the average was taken.

3.8. Mass Spectrometry Analysis of the Structure of the Purified DHP Compounds

The molecular weights of compounds G_1, G_2, G_3, and GS_1 were determined by high-performance benchtop quadrupole trap atmospheric pressure chemical ionisation mass spectrometry (APCI-MS) (Q Exactive HR MS, Thermo Fisher Scientific, Waltham, MA, USA) [62–64]. The scanning range of the ion source was m/z 70–1050. Nitrogen was used as a drying gas and the flow rate was 45 mL/min.

4. Conclusions

1. DHP-G and DHP-GS were synthesised by laccase-catalysed dehydrogenation polymerisation. The ^{13}C-NMR spectra showed that both DHP-G and DHP-GS contained β-O-4, β-5, β-β, β-1, and 5-5 substructures.
2. The ether-soluble fractions C_{12} of DHP-G and C_{22} of DHP-GS had strong antibacterial activities against *E. coli* and *S. aureus*.
3. The antibacterial activities of compounds GS_1–GS_5 purified from the C_{22} fraction and compounds G_1–G_5 separated from the C_{12} fraction were stronger against *E. coli* than *S. aureus*. The separated compounds G_1, G_2, G_3, and GS_1 had strong inhibitory effects against *E. coli* and *S. aureus*.
4. According to the results of APCI-MS, compound G_1 was a (β-5) G-type dimer, while compound G_2 was a (β-5) (β-5) G-type trimer, and G3 was a (β-O-4) (β-5) (β-5) G-type tetramer. GS_1 was a (β-5) GS-type dimer.

5. Higher molecular weight and the introduction of syringyl units reduced the antibacterial activity. The antibacterial activity of G_1, which had the best antibacterial activity, is attributable to the β-5-type connected phenylcoumaran dimer.

Author Contributions: Data curation, X.W.; Methodology, X.W.; Writing—original draft preparation, X.W.; Formal analysis, S.C.; Supervision, S.C. and Y.X.; Funding acquisition, Y.X.; Writing—review and editing, Y.X. All authors have read and agreed to the published version of the manuscript.

Funding: This research was funded by the National Natural Science Foundation of China (Grant No. 21878070), and the Outstanding Young and Middle-aged Technological Innovation Team Project of Hubei Provincial Universities (Grant No. T201205).

Institutional Review Board Statement: Not applicable.

Informed Consent Statement: Not applicable.

Data Availability Statement: The data presented in this study are available in the manuscript.

Conflicts of Interest: The authors declare no conflict of interest.

Sample Availability: Samples of the compounds are not available from the authors.

References

1. Brianna, M.; Andrea, M. Strategies for the Conversion of Lignin to High-Value Polymeric Materials: Review and Perspective. *Chem. Rev.* **2016**, *116*, 2275–2306.
2. Gillet, S.; Aguedo, M.; Petitjean, L.; Morais, A.R.C.; Costa Lopes, A.M.D.; Łukasik, R.M.; Anastas, P.T. Lignin Transformations for High Value Applications: Towards Targeted Modifications Using Green Chemistry. *Green Chem.* **2017**, *19*, 4200–4233. [CrossRef]
3. Parit, M.; Jiang, Z. Towards lignin derived thermoplastic polymers. *Biol. Macromol.* **2020**, *165*, 3180–3197. [CrossRef]
4. Fortunati, E.; Yang, W.; Luzi, F.; Kenny, J.; Torre, L.; Puglia, D. Lignocellulosic nanostructures as reinforcement in extrudedand solvent casted polymeric nanocomposites: An overview. *Eur. Polym.* **2016**, *80*, 295–316. [CrossRef]
5. Wu, W.; Dutta, T.; Varman, A.M.; Eudes, A.; Manalansan, B.; Loqué, D.; Singh, S. Lignin valorization: Two hybrid biochemical routes for the conversion of polymeric lignin into value-added chemicals. *Sci. Rep.* **2017**, *7*, 8420. [CrossRef] [PubMed]
6. Figueiredo, P.; Lintinen, K.; Hirvonen, J.T.; Kostiainen, M.A.; Santos, H.A. Properties and chemical modifications of lignin: Towards lignin-based nanomaterials for biomedical applications. *Prog. Mater. Sci.* **2018**, *93*, 233–269. [CrossRef]
7. Sláviková, E.; Košíková, B. Inhibitory effect of lignin by-products of pulping on yeast growth. *Folia Microbiol.* **1994**, *39*, 241–243. [CrossRef]
8. Thakur, V.K.; Thakur, M.K. Recent advances in green hydrogels from lignin: A review. *Biol. Macromol.* **2015**, *72*, 834–847. [CrossRef]
9. Asina, F.; Brzonova, I.; Kozliak, E.; Kubátová, A.; Jin, Y. Microbial treatment of industrial lignin: Successes, problems and challenges. *Renew. Sustain. Energy Rev.* **2017**, *77*, 1179–1205. [CrossRef]
10. Guo, M.; Tony, J.; Nghiem, N.P.; Fan, X.; Phoebe, X.Q.; Jang, C.; Shao, L.; Wu, C. Assessment of Antioxidant and Antimicrobial Properties of Lignin from Corn Stover Residue Pretreated with Low-Moisture Anhydrous Ammonia and Enzymatic Hydrolysis Process. *Appl. Biochem. Biotechnol.* **2018**, *184*, 350–365. [CrossRef]
11. Maia, R.A.; Ventorim, G.; Batagin-Neto, A. Reactivity of lignin subunits: The influence of dehydrogenation and formation of dimeric structures. *Mol. Model.* **2019**, *25*, 228. [CrossRef] [PubMed]
12. Feneley, R.C.L.; Hopley, I.B.; Wells, P.N.T. Urinary catheters: History, current status, adverse events and research agenda. *Med. Eng. Technol.* **2015**, *39*, 459–470. [CrossRef] [PubMed]
13. Domínguez-Robles, J.; Larrañeta, E.; Fong, M.L.; Martin, N.K.; Irwin, N.J.; Mutjé, P.; Tarrés, P.; Delgado-Aguilar, M. Lignin/Poly (bu-tylene succinate) composites with antioxidant and antibacterial properties for potential biomedical applications. *Biol. Macromol.* **2020**, *145*, 92–99. [CrossRef] [PubMed]
14. Kaur, R.; Uppal, S.K.; Sharma, P. Antioxidant and Antibacterial Activities of Sugarcane Bagasse Lignin and Chemically Modified Lignins. *SugarTech* **2017**, *19*, 675–680. [CrossRef]
15. Freudenberg, K.; Hübner, H.H. Oxyzimtalkohole und ihre Dehydrierungs polymerisate. *Chem. Ber.* **1952**, *85*, 1181–1191. [CrossRef]
16. Zheng, L.; Lu, G.; Pei, W.; Yan, W.; Li, Y.; Zhang, L.; Huang, C.; Jiang, Q. Understanding the relationship between the structural properties of lignin and their biological activities. *Biol. Macromol.* **2021**, *190*, 291–300. [CrossRef]
17. Xu, Y.; Zeng, P.; Li, M.; Bian, J.; Peng, F. γ-Valerolactone/water system for lignin fractionation to enhance antibacterial and antioxidant capacities. *Sep. Purif. Technol.* **2021**, *279*, 119780. [CrossRef]
18. Rocca, D.M.; Vanegas, J.P.; Fournier, K.; Becerra, M.C.; Scaiano, J.C.; Lanterna, A.E. Biocompatibility and photo-induced antibacterial activity of lignin-stabilized noble metal nanoparticles. *RSC Adv.* **2018**, *8*, 40454–40463. [CrossRef]

19. Marulasiddeshwara, M.B.; Dakshayani, S.S.; Kumar, M.N.S.; Chethana, R.; Kumar, P.R.; Devaraja, S. Facile-one pot-green synthesis, antibacterial, antifungal, antioxidant and antiplatelet activities of lignin capped silver nanoparticles: A promising therapeutic agent. *Mater. Sci. Eng. C* **2017**, *81*, 182–190. [CrossRef]
20. Lourençon, T.V.; de Lima, G.G.; Ribeiro, C.S.; Hansel, F.A.; Maciel, G.M.; da Silva, K.; Winnischofer, S.M.B.; de Muniz, G.I.B.; Magalhães, W.L.E. Antioxidant, antibacterial and antitumoural activities of kraft lignin from hardwood fractionated by acid precipitation. *Biol. Macromol.* **2021**, *166*, 1535–1542. [CrossRef]
21. Guan, S.; Mlynár, J.; Sarkanen, S. Dehydrogenative polymerization of conifery alcohol on macromolecular lignin templates. *Phytochemistry* **1997**, *45*, 911–918.
22. Terashima, N.; Atalla, R.H.; Ralph, S.A.; Landucci, L.L.; Lapierre, C.; Monties, B. New Preparations of Lignin Polymer Models under Conditions that Approximate Cell Wall Lignification. I. Synthesis of Novel Lignin Polymer Models and their Structural Characterization by ^{13}C NMR. *Holzforschung* **1995**, *49*, 521–527. [CrossRef]
23. Fournand, D.; Cathala, B.; Lapierre, C. Initial steps of the peroxidase-catalyzed polymerization of coniferyl alcohol and/or sinapyl aldehyde: Capillary zone electrophoresis study of pH effect. *Phytochemistry* **2003**, *62*, 139–146. [CrossRef]
24. Yanez, A.J.; Li, W.; Mabon, R.; Broadbelt, L.J. A Stochastic Method to Generate Libraries of Structural Representations of Lignin. *Energy Fuels* **2016**, *30*, 5835–5845. [CrossRef]
25. Zhao, Z.; Liu, Z.; Pu, Y.; Meng, X.; Xu, J.; Yuan, J.; Ragauskas, A.J. Emerging Strategies for Modifying Lignin Chemistry to Enhance Biological Lignin Valorization. *ChemSusChem* **2020**, *20*, 5423–5432. [CrossRef]
26. Shu, F.; Jiang, B.; Yuan, Y.; Li, M.; Wu, W.; Jin, Y.; Xiao, H. Biological Activities and Emerging Roles of Lignin and Lignin-Based Products—A Review. *Biomacromolecules* **2021**, *22*, 4905–4918. [CrossRef]
27. Ye, Z.; Xie, Y.; Wu, C.; Wang, P.; Le, X. Dehydrogenation polymerization of isoeugenol and formation of lignin-carbohydrate complexes with presence of polysaccharide. *Chem. Ind. For. Prod.* **2016**, *36*, 45–50.
28. Salanti, A.; Orlandi, M.; Tolppa, E.L.; Zoia, L. Oxidation of Isoeugenol by Salen Complexes with Bulky Substituents. *Int. J. Mol. Sci.* **2010**, *11*, 912–926. [CrossRef]
29. Chen, X.; Zhao, H.; Wu, H.; Ye, Z.; Xie, Y. Preparation and antioxidant properties of dehydrogenation polymer of isoeugenol. *Chem. Ind. For. Prod.* **2018**, *38*, 87–92.
30. Xie, Y.; Yasuda, S.; Wu, H.; Liu, H. Analysis of the structure of lignin-carbohydrate complexes by the specific ^{13}C tracer method. *Wood Sci.* **2000**, *46*, 130–136. [CrossRef]
31. Holtman, K.M.; Chang, H.; Kadla, J.F. Solution-state nuclear magnetic resonance study of the similarities between milled wood lignin and cellulolytic enzyme lignin. *Agric. Food Chem.* **2004**, *52*, 720–726. [CrossRef] [PubMed]
32. Lindfors, C.; Mäki-Arvela, P.; Paturi, P.; Aho, A.; Eränen, K.; Hemming, J.; Peurla, M.; Kubička, D.; Simakova, I.L.; Murzin, D.Y. Hydrodeoxygenation of Isoeugenol over Ni- and Co-Supported Catalysts. *ACS Sustain. Chem. Eng.* **2019**, *7*, 14545–14560. [CrossRef]
33. Ahn, J.; Avonto, C.; Chittiboyina, A.G.; Khan, I.A. Is Isoeugenol a Prehapten? Characterization of a Thiol-Reactive Oxidative Byproduct of Isoeugenol and Potential Implications for Skin Sensitization. *Chem. Res. Toxicol.* **2020**, *33*, 948–954. [CrossRef] [PubMed]
34. Hage, R.E.; Brosse, N.; Chrusciel, L.; Sanchez, C.; Sannigrahi, P.; Ragauskas, A. Characterization of milled wood lignin and ethanol organosolv lignin from miscanthus. *Polym. Degrad. Stab.* **2009**, *94*, 1632–1638. [CrossRef]
35. Lüdemann, H.D.; Nimz, H.H. Carbon-13 nuclear magnetic resonance spectra of lignins. *Biochem. Biophys. Res. Commun.* **1973**, *52*, 1162–1169. [CrossRef]
36. Nimz, H.H.; Tschirner, U.; Stähle, M.; Lehmann, R.; Schlosser, M. Carbon-13 NMR Spectra of Lignins, 10.[1] Comparison of Structural Units in Spruce and Beech Lignin. *Wood Chem. Technol.* **1984**, *4*, 265–284. [CrossRef]
37. McElroy, R.D.; Lai, K. Fractionation-purification, IR, ^{1}H ^{13}C NMR spectral and property studies of an industrial based sludge lignin. *Wood Chem. Technol.* **1988**, *8*, 361–378. [CrossRef]
38. Xie, Y.; Robert, D.R.; Terashima, N. Selective carbon 13 enrichment of side chain carbons of ginkgolignin traced by carbon 13 nuclear magnetic resonance. *Plant Physiol. Biochem.* **1994**, *32*, 243–249.
39. Harman-Ware, A.E.; Happs, R.M.; Davison, B.H.; Davis, M.F. The effect of coumaryl alcohol incorporation on the structure and composition of lignin dehydrogenation polymers. *Biotechnol. Biofiuels* **2017**, *10*, 281. [CrossRef]
40. Xie, Y.; Terashima, N. Selective Carbon 13-Enrichment of Side Chain Carbons of Ginkgo Lignin Traced by Carbon 13 Nuclear Magnetic Resonance*. *Mokuzai Gakkaishi* **1991**, *37*, 935–941.
41. Lapierre, C.; Monties, B.; Guittet, E.; Lallemand, J.Y. Photosynthetically ^{13}C-Labelled Poplar Lignins: ^{13}C NMR Experiments. *Gruyter* **1984**, *38*, 333–342.
42. Choi, J.W.; Faix, O. NMR study on residual lignins isolated from chemical pulps of beech wood by enzymatic hydrolysis. *Ind. Eng. Chem.* **2011**, *17*, 25–28. [CrossRef]
43. Xie, Y.; Chen, X.; Zhao, H.; Jiang, C.; Wu, H.; Bi, S.; Ye, Z. Preparation of dehydrogenation polymer from isoeugenol and biological activity characterization. In *Biochemistry Research Trends*; Lu, F., Yue, F., Eds.; Nova Science Publishers Inc.: New York, NY, USA, 2019; pp. 281–296.
44. Benhabiles, M.S.; Salah, R.; Lounici, H.; Drouiche, N.; Goosen, M.F.A.; Mameri, N. Antibacterial activity of chitin, chitosan and its oligomers prepared from shrimp shell waste. *Food Hydrocoll.* **2012**, *29*, 48–56. [CrossRef]

45. Brown, J.S.; Mohamed, Z.J.; Artim, C.M.; Thornlow, D.N.; Hassler, J.F.; Rigoglioso, V.P.; Daniel, S.; Alabi, C.A. Antibacterial isoamphipathic oligomers highlight the importance of multimeric lipid aggregation for antibacterial potency. *Commun. Biol.* **2018**, *1*, 220. [CrossRef] [PubMed]
46. Grace, J.L.; Schneider-Futschik, E.K.; Elliott, A.G.; Amado, M.; Truong, N.P.; Cooper, M.A.; Li, J.; Davis, T.P.; Quinn, J.F.; Velkov, T.; et al. Exploiting macromolecular design to optimize the antibacterial activity of alkylated cationic oligomers. *Biomacromolecules* **2018**, *19*, 4629–4640. [CrossRef]
47. Shaikh, F.; Shastri, S.L.; Naik, N.S.; Kulkarni, R.; Madar, J.M.; Shastri, L.A.; Joshi, S.D.; Sunagar, D.V. Synthesis, Antitubercular and Antimicrobial Activity of 1,2,4-Triazolidine-3-thione Functionalized Coumarin and Phenyl Derivatives and Molecular Docking Studies. *Chem. Chem.* **2019**, *4*, 105–115. [CrossRef]
48. Christofferson, A.J.; Elbourne, A.; Cheeseman, S.; Shi, Y.; Rolland, M.; Cozzolino, D.; Chapman, J.; McConville, C.F.; Crawford, R.J.; Wang, P.; et al. Conformationally tuned antibacterial oligomers target the peptidoglycan of Gram-positive bacteria. *Colloid Interface Sci.* **2020**, *580*, 850–862. [CrossRef]
49. Senioa, S.; Pereira, C.; Vaz, J.; Sokovic, M.; Barros, L.; Ferreira, I.C.F.R. Dehydration process influences the phenolic profile, antiox idant and antimicrobial properties of *Galium aparine* L. *Ind. Crops Prod.* **2018**, *120*, 97–103. [CrossRef]
50. Xie, Y.; Chen, X.; Jiang, C.; Wu, H.; Ye, Z. Preparation of oligomeric dehydrogenation polymer and characterization of its antibacterial properties. *Bioresources* **2019**, *14*, 2842–2860.
51. Hattori, M.; Hada, S.; Watahiki, A.; Ihara, H.; Shu, Y.; Kakiuchi, N.; Mizuno, T.; Namba, T. Studies on dental caries prevention by traditional medicines. X. Antibacterial action of phenolic compounds from mace against Streptcoccus mutans. *Chem. Pharm. Bull.* **1986**, *34*, 3885–3893. [CrossRef]
52. Dinev, Z.; Wardak, A.Z.; Brownlee, R.T.C.; Williams, S.J. A convenient gram-scale synthesis of uridine diphospho (^{13}C6) glucose. *Carbohydr. Res.* **2006**, *341*, 1743–1747. [CrossRef] [PubMed]
53. Wang, K.; Xu, F.; Sun, R. Molecular characteristics of kraft-AQ pulping lignin fractionated by sequential organic solvent extraction. *Int. J. Mol. Sci.* **2010**, *11*, 2988–3001. [CrossRef] [PubMed]
54. Li, M.F.; Sun, S.N.; Xu, F.; Sun, R.C. Sequential solvent fractionation of heterogeneous bamboo organosolv lignin for value-added application. *Sep. Purif. Technol.* **2012**, *101*, 18–25. [CrossRef]
55. Tan, C.; Kong, L.; Li, X.; Li, W.; Li, N. Isolation and analysis of a new phytoecdysteroid from Cyanotis arachnoidea C. B. Clarke. *Chin. J. Chromatogr.* **2011**, *29*, 937–941.
56. Xiang, Y. Introduction of column chromatography for mixture separation. *Chin. J. Chem. Educ.* **2015**, *36*, 1–3.
57. Carovic-Stanko, K.; Orlic, S.; Politeo, O.; Strikić, F.; Kolak, I.; Milos, M.; Satovic, Z. Composition and antibacterial activities of essential oils of seven Ocimum taxa. *Food Chem.* **2010**, *119*, 196–201. [CrossRef]
58. Zhang, C.X.; Qiao, X.M.; Chen, H.W.; Zhang, Y.Y. Syntheses and Biological Activities of Lanthanide Metal Complexes with Nitronly Nitroxide. *Synth. React. Inorg. Met. Org. Nano-Met. Chem.* **2015**, *45*, 145–150. [CrossRef]
59. Choi, O.; Cho, S.K.; Kim, J.; Park, C.G.; Kim, J. In vitro antibacterial activity and major bioactive components of Cinnamomum verum essential oils against cariogenic bacteria, Streptococcus mutans and Streptococcus sobrinus. *Asian Pac. J. Trop. Biomed.* **2016**, *6*, 308–314. [CrossRef]
60. Jain, S.; Bhanjana, G.; Heydarifard, S.; Dilbaghi, N.; Nazhad, M.M.; Kumar, V.; Kim, K.; Kumar, S. Enhanced antibacterial profile of nanoparticle impregnated cellulose foam filter paper for drinking water filtration. *Carbohydr. Polym.* **2018**, *202*, 219–226. [CrossRef]
61. Owuama, C.I. Determination of minimum inhibitory concentration (MIC) and minimum bactericidal concentration (MBC) using a novel dilution tube method. *Afr. J. Microbiol. Res.* **2017**, *11*, 977–980.
62. Evtuguin, D.V.; Amado, F.M.L. Application of electrospray ionization mass spectrometry to the elucidation of the primary structure of lignin. *Macromol. Biosci.* **2003**, *3*, 339–343. [CrossRef]
63. Reale, S.; Tullio, A.D.; Spreti, N.; Angelis, F.D. Mass spectrometry in the biosynthetic and structural investigation of lignins. *Mass Spectrom. Rev.* **2004**, *23*, 87–126. [CrossRef] [PubMed]
64. Brecht, D.; Uteschil, F.; Schmitz, O.J. Development of a fast-switching dual (ESI/APCI) ionization source for liquid chromatography/mass spectrometry. *Rapid Commun. Mass Spectrom.* **2020**, *34*, e8845. [CrossRef] [PubMed]